

# Agile 3D-Navigation of a Helical Magnetic Swimmer

Julien Leclerc<sup>1</sup>, Haoran Zhao<sup>1</sup>, Daniel Z. Bao<sup>1</sup>, Aaron T. Becker<sup>1</sup>, Mohamad Ghosn<sup>2</sup> and Dipan J. Shah<sup>2</sup>

**Abstract**—Rotating miniature magnetic swimmers are devices that could navigate within the bloodstream to access remote locations of the body and perform minimally invasive procedures. The rotational movement could be used, for example, to abrade a pulmonary embolus. Some regions, such as the heart, are challenging to navigate. Cardiac and respiratory motions of the heart combined with a fast and variable blood flow necessitate a highly agile swimmer. This swimmer should minimize contact with the walls of the blood vessels and the cardiac structures to mitigate the risk of complications. This paper presents experimental tests of a millimeter-scale magnetic helical swimmer navigating in a blood-mimicking solution and describes its turning capabilities. The step-out frequency and the position error were measured for different values of turn radius. The paper also introduces rapid movements that increase the swimmer’s agility and demonstrates these experimentally on a complex 3D trajectory.

## I. INTRODUCTION

Acute pulmonary embolism (PE) is a worldwide problem that afflicts a large number of individuals (approximately 6 persons per 10,000 and per year [1]). Most PEs originate from a thrombus (blood clot) in the lower extremities which dislodges and migrates to the lungs. The sequelae (long term consequences) of PE are predominantly due to anatomical obstruction of blood flow through the pulmonary arteries, which results in increased afterload on the right ventricle of the heart. This can potentially result in death from massive right ventricular failure and/or arrhythmia.

Anticoagulants are the mainstay of treatment for submassive PE; however, the hemodynamic instability associated with massive PE warrants more urgent treatment. Thrombolysis involves administration of pharmacologic therapy which can dissolve thrombus. However, systemic administration of thrombolytic medication can be complicated by life-threatening bleeding in 0.6% of cases [2]. Outcomes can be improved by using catheters to deliver thrombolytic medication locally. An ultrasound transducer placed at the tip of the catheter is sometimes used to speed up thrombolysis [3]. The thrombus can also be removed using an aspiration tool with the catheter [4]. This procedure requires the availability of interventional procedural suites and skilled

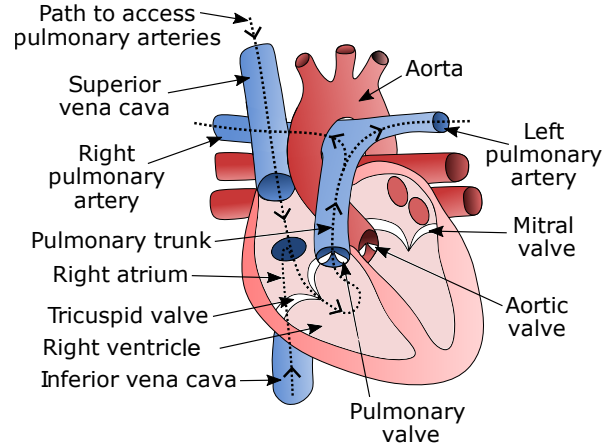


Fig. 1. Schematic representation of a human heart. Dashed lines show representative paths that a magnetic swimmer entering via the superior vena cava could follow to reach the pulmonary arteries.

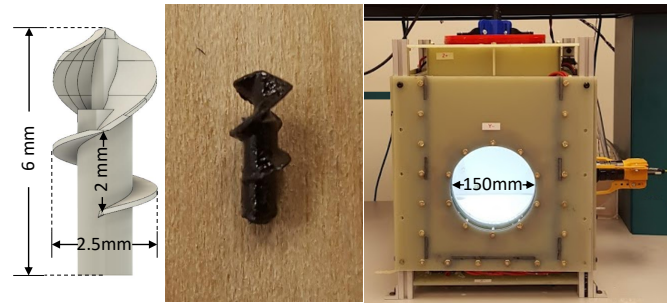


Fig. 2. CAD drawing (left) and picture of the helical swimmer (center). Picture of the magnetic manipulator used in this study (right).

interventionalist physicians. This is routinely not available at small community-based hospitals where most of these patients initially present. The ability of more widespread emergent thrombolysis without incurring the risk of bleeding from pharmacologic thrombolytic therapy is highly desirable. A tiny tetherless device capable of rapidly accessing a remote PE, destroying the clot, and exiting the body could transform treatment paradigms.

Navigating tetherless agents within the human body as in Fig. 1, instead of inserting catheters could improve the patient’s outcome. Magnetic agents would not need an onboard power supply, sensors or processor and would therefore be relatively easy to miniaturize.

The device investigated in this paper is a helical rotating magnetic swimmer, shown in Fig. 2. This agent is composed of a radially magnetized permanent magnet embedded into a helical body. When a rotating magnetic field is applied, the agent rotates. The helical shape converts the rotational

\*Work supported by NSF IIS-1553063, CNS-1646566, and CNS-1932572

\*Dr. Shah receives salary support from the National Science Foundation (grants CNS-1646566 and CNS-1931884) and the National Institutes of Health (1R01HL137763-01)

(1) Department of Electrical Engineering, University of Houston, 4800 Calhoun Rd, Houston, TX 77004, USA

(2) Houston Methodist DeBakey Heart & Vascular Center, 6550 Fannin Street, Houston, TX 77030, USA

jleclerc@central.uh.edu, hzhao9@central.uh.edu,  
atbecker@central.uh.edu, mghosn@houstonmethodist.org,  
djshah@houstonmethodist.org

movement into a propulsive force. These swimmers can follow a path in 3D [5]–[7] and use their rotational movement to abrade blood clots [8]–[11].

To treat PE, the swimmer will first be inserted inside a blood vessel. Methods similar to those used to insert central catheters and intravenous lines could be re-used for this purpose. Once inserted the swimmer will navigate toward the embolus. It will enter the heart right atrium via the superior or inferior vena cava, depending on the vein it is inserted into (see Fig. 1). It will then traverse the tricuspid valve to enter the right ventricle and exit this chamber via the pulmonary valve. This valve leads to the pulmonary trunk. The swimmer will then continue the navigation downstream and access either the left or right pulmonary artery, depending on the location of the embolus. The swimmer’s tip can be used as a rotating tool to abrade the clot. It is likely that the retrieval location of the swimmer will be the same as the insertion location. The swimmer will therefore have to navigate the previous path in a retrograde fashion to reach the retrieval location after treatment of the PE.

This trajectory is challenging to execute:

- The heart as well as the vessels move and the swimmer will have to avoid collisions with the surrounding tissue.
- The blood flow inside the heart is high and variable. The swimmer will have to counteract this flow and rapidly react to the changes of flow speed.
- The swimmer will have to go through heart valves and avoid touching them.

A highly agile swimmer will be essential to the success of this navigation. The swimmer must be able to quickly change its velocity direction and magnitude to adapt to this highly dynamic environment. It is, however, important that the control commands stay within the capability range of the system. For example, if the magnetic field direction is changed too quickly, the angle between the applied field and the magnetization of the swimmer ( $\theta_i$ ) could exceed  $\pi/2$ . The torque applied to the swimmer is (1).

$$\Gamma = \Gamma_{\max} \cdot \sin(\theta_i). \quad (1)$$

Torque is maximized when  $\theta_i = \pi/2$ . However, if  $\theta_i$  exceeds  $\pi/2$ , any further increase decreases the applied torque. This leads to a situation where the controller will request a torque that is greater than the maximum capabilities of the system. When this happens in our experimental apparatus, the swimmer simply stops rotating and falls to the bottom of the workspace. The rotational frequency that leads to an angle  $\theta_i = \pi/2$  is called the *step-out frequency*. Sometimes a swimmer may continue to rotate above the step-out frequency [12]. This behavior was not observed during our experiments. Our swimmer abruptly stops rotating when the step-out frequency is exceeded.

This paper experimentally investigates the agility of a helical swimmer. This information has high importance for surgical applications as it enables predicting if a planned navigation is within the capabilities of the system or not. It will also help to ensure that the control commands do

not exceed the maximum values for stable and accurate navigation.

The term *agility* has been used with different meanings in many fields, including robotics, sports and psychology. Eckert and Ijspeert explained that “the agility of a system or a being is hard to grasp, measure and quantify” [13]. In our study, the term *agility* refers to the ability of the swimmer to rapidly change its velocity vector and/or its orientation while keeping a low position error on the trajectory followed. High agility requires proper design and tuning of all components of a device to ensure that all the subsystems work in coordination.

Section II presents the experimental apparatus used in this study. Subsection III-A investigates the ability of the swimmer to perform fast turns. In Subsection III-B the step-out frequency is measured as a function of the turning radius. Section IV introduces special movements that enable performing highly agile maneuvers. Section VI discusses conclusions about this work.

## II. EXPERIMENTAL APPARATUS

### A. Magnetic manipulator

The hardware used for the experiment was thoroughly described in [14] and will only be briefly described here. The system is a small-size laboratory manipulator and is not large enough to accommodate a person. A larger device would need to be used for human surgery. The system possesses six electromagnets (EM) that have an internal diameter of 150 mm and are placed in a cubic shape. The swimmer navigates in a water tank placed in the middle of the EM assembly. The EM are powered by twelve KEPCO BOP 50-20 MG. Each EM is connected to a set of two power supplies connected in series. Their current is controlled via an analog input. Two Basler cameras placed at an angle of 90 degrees are used to measure the position of the swimmer. The images are processed by an industrial controller IC-3173 manufactured by National Instruments. This controller also performs all control computation for the swimmer (see description of the algorithm in Section II-D). It was programmed using LabVIEW.

### B. Magnetic swimmer

The same magnetic swimmer was used for all the experiments presented in this paper. A picture and a CAD drawing of this swimmer are presented in Fig. 2.

The swimmer geometry was selected after testing 16 different designs. The swimmers were tested navigating inside the blood-mimicking solution described in subsection II-C. The presented design was selected for its overall swimming qualities (stability, velocity, possible rotational speed range).

The swimmer has an external diameter of 2.5 mm and a length of 6 mm. It has the shape of an helix at its fore side. The helix has a pitch of 2 mm and covers 75% of the length of the swimmer. The swimmer was 3D-printed using a ProJet 3510 HD. The aft side of the swimmer has the shape of a hollow tube in which a cylindrical NdFeB permanent magnet is inserted. The permanent magnet has a length of 1

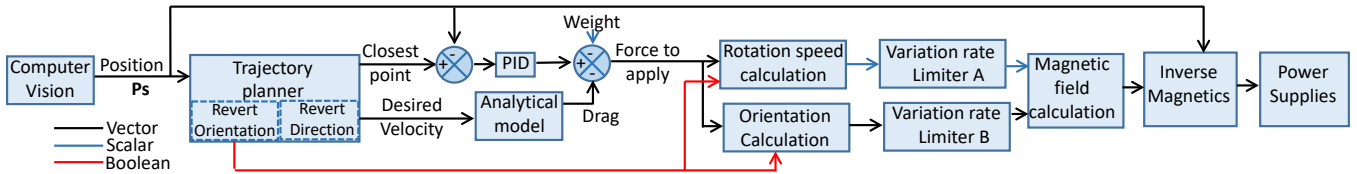


Fig. 3. Block diagram presenting the structure of the controller used in this study.

mm, a diameter of 0.75 mm, and is radially magnetized. The permanent magnet can be completely encapsulated into the helical body and epoxy resin to avoid contact with blood.

### C. Blood-mimicking solution

All experiments were performed in a solution of 27.5% glycerol and 10% ethyl alcohol mixed with distilled water. The liquid was at room temperature during the experiments.

The viscosity of this solution was measured using an OF-ITE Model 900 viscometer at 100 turns/min (corresponding to a shear rate of  $170 \text{ s}^{-1}$ ) and is equal to  $3.10 \times 10^{-3} \text{ Pa}\cdot\text{s}^{-1}$ . Newtonian models for blood often assume a viscosity equal to  $3.5 \times 10^{-3} \text{ Pa}\cdot\text{s}^{-1}$  [15]. For comparison, water viscosity is equal to  $8.9 \times 10^{-4} \text{ Pa}\cdot\text{s}^{-1}$ . Blood viscosity depends on the hematocrit of the individual. Blood also exhibits a complex rheological behaviour that is not only shear-dependent but also time-dependent [16]. The solution used does not fully reflect this complexity, but its viscosity is within the range of measured values for human blood [17].

The relative density (compared to water) of the solution was measured using a hydrometer and is equal to 1.05, which is a normal value for human blood [18].

### D. Controller

The controller presented in [19] was modified to be able to perform the maneuvers described in Section IV.

The trajectory planner (TP, see Fig. 3) receives as input the position of the swimmer and searches for the closest point on the trajectory and the desired velocity vector at this location. The location of the closest point is compared to the actual position and the difference is sent to a PID regulator to keep the swimmer close to the trajectory centerline. The desired velocity is sent to an analytical model that predicts the drag of the swimmer. The TP was modified and now sends a Boolean value to the orientation calculation module (OCM). When this variable is set to true, the orientation of the swimmer is flipped. This is performed in the OCM by multiplying the orientation vector by  $-1$ . This Boolean value is also sent to the module calculating the rotational speed to request a change of the rotational direction (see Subsection IV-B).

The TP is also now able to generate a negative desired velocity output. The sign of this variable determines the direction followed by the swimmer along the path. Abruptly changing this variable from a positive to a negative value causes the swimmer to quickly change direction (see Subsections IV-A and IV-C).

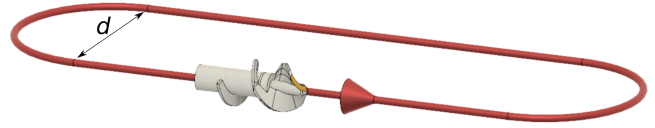


Fig. 4. Image showing the racetrack-shaped trajectory used to study the steering abilities of the swimmer (swimmer not to scale).

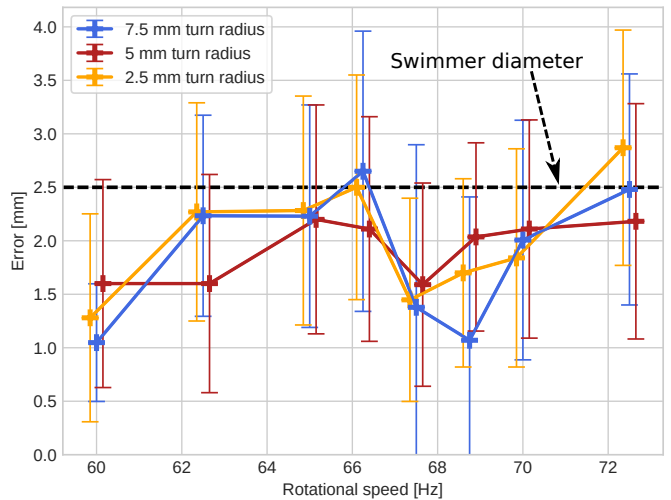


Fig. 5. The average swimmer position error while turning with radii of 7.5, 5 and 2.5 mm, is less than the swimmer diameter for all but two tests. Data points were recorded every 15 ms for 5 turns with each combination. The error bars represent the standard deviation of the measured data.

## III. STEERING CAPABILITIES

This section experimentally measures the position error while steering as a function of turning radius, and measures the step-out frequency as a function of turning radius.

### A. Position error while steering

For this experiment, the swimmer was programmed to navigate a racetrack-shaped trajectory placed in the horizontal plane at  $z = 0$  (see Fig. 4). The swimmer was rotating at a constant speed along the trajectory. The navigation was performed for three turn radii and for eight rotational speeds.

The positioning error is calculated using (2), where  $x$ ,  $y$  and  $z$  are the coordinates of the position of the swimmer and  $x_c$ ,  $y_c$  and  $z_c$  are the coordinates of the closest point of the trajectory.

$$E = \sqrt{(x - x_c)^2 + (y - y_c)^2 + (z - z_c)^2} \quad (2)$$

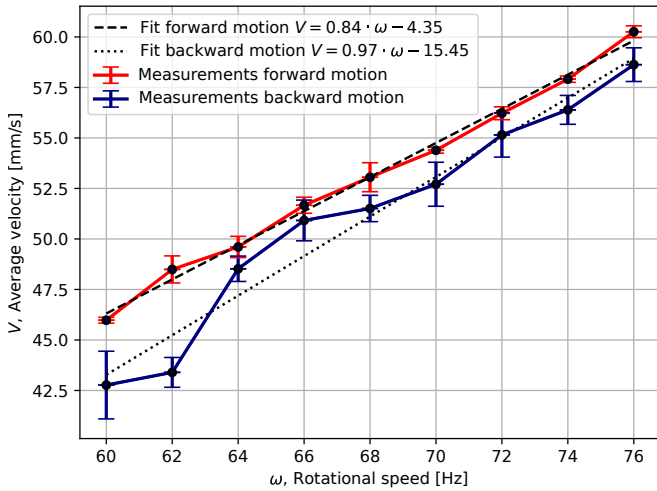


Fig. 6. Average velocity of the swimmer while performing a  $180^\circ$  turn as a function of the rotational frequency. The turning radius was 7.5 mm. The forward and backward curves are approximated by the shown linear fits with coefficients of determination  $R^2_{\text{forward}}=0.995$  and  $R^2_{\text{backward}}=0.96$ .

This error was computed and stored at intervals of 15 ms and over 5 trials. Results of these measurements for turn radii equal to 7.5, 5 and 2.5 mm are presented in Fig. 5. The error, plotted as a function of the rotational speed, follows the same trend for each turn radius. The error mostly tends to increase with the rotational speed. The plots also present a local minimum between  $f=67$  Hz and 69 Hz. This complex behavior could be the result of several opposing effects. For example, at low speeds, the controller has more time to correct the trajectory before the error accumulates. Conversely, a reduced rotational speed means a reduced propulsive force and therefore a reduced control authority. The error bars on Fig. 5 are large in comparison to the variation of the average value. Error bars represent the standard deviation of the measured values. This data dispersion is not caused by a measurement error but by the system's imprecision. In this experiment the position measurement system has a resolution of approximately 0.1 mm in the  $xy$  plane, while the standard deviation is approximately  $\pm 1$  mm.

The velocity of the swimmer was measured while performing a continuous 7.5 mm radius turn. Results are presented in Fig. 6. The forward velocity  $V$  is approximately a linear function of the rotational speed  $\omega$  and can be approximated by  $V = 0.84 \cdot \omega - 4.35$  with  $R^2_{\text{forward}}=0.995$ . The backward velocity is slower and can be approximated by  $V = 0.97 \cdot \omega - 15.45$  with  $R^2_{\text{backward}}=0.96$ . The difference in speed ranges from 7% of the forward speed at 60 Hz to 2% of the speed at 76 Hz. This difference in speed makes flipping the swimmer and moving tip first faster than backing-up the swimmer for a long backwards path.

### B. Step-out frequency during steering

During the previous experiment, it was observed that the step-out frequency was only detected during turns. Exceeding the step-out frequency in our experiment results in the

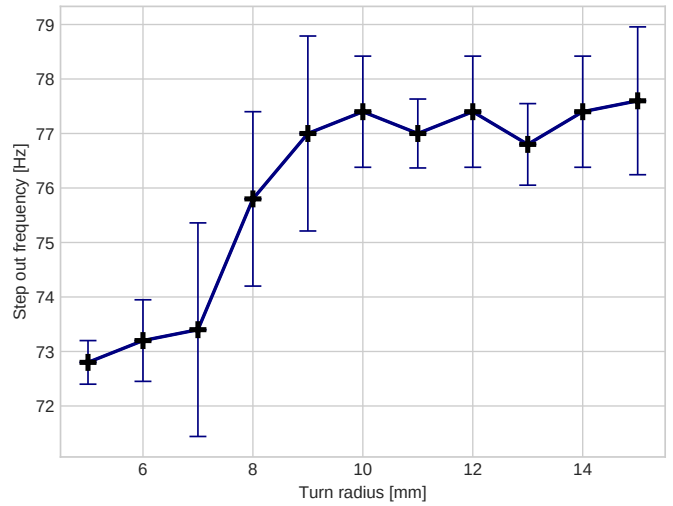


Fig. 7. Step-out frequency as a function of the turn radius for forward movement. Each data point represents five trials. The error bars represent the standard deviation of the measured data.

swimmer stopping rotating and falling to the bottom of the workspace. Turning increases the torque required to move the swimmer, and this decreases the step-out frequency.

The step-out frequency was measured as a function of the turning radius. Results are plotted in Fig. 7 and show that the step-out frequency is a function of the turning radius and decreases at lower radii.

## IV. SPECIAL RAPID MOVEMENTS

This section introduces special movements that can produce rapid changes of the velocity or orientation of the swimmers. These movements either involve a  $180^\circ$  change of the swimmer orientation or the reversal of its rotational direction. They could be useful during certain phases of the navigation. For example, the sharp turn that needs to be made inside the right ventricle of the heart could be accomplished rapidly by executing the movement described in Subsections IV-A and IV-C.

### A. Direction reversal

This maneuver is executed by having the TP instantaneously change the sign of the desired velocity (see Fig. 3). The variation rate limiter  $A$  limits the swimmer's rotational speed change rate to a constant value, set to  $10,000 \text{ rad/s}^2$  in our experiment. The swimmer was programmed to follow a straight horizontal line and perform a direction reversal maneuver at each end until the program is manually stopped. A video of this experiment is attached to this paper [20]. Frames from the video as well as a plot of the experimental trajectory are presented in Fig. 8.

### B. Orientation reversal

For this maneuver the TP sends orientation change requests to the OCM (see Fig. 3). The OCM then internally multiplies the orientation vector by  $-1$  to invert its orientation. This has the effect of flipping the orientation of the swimmer. The variation rate limiter  $B$  limits the variation

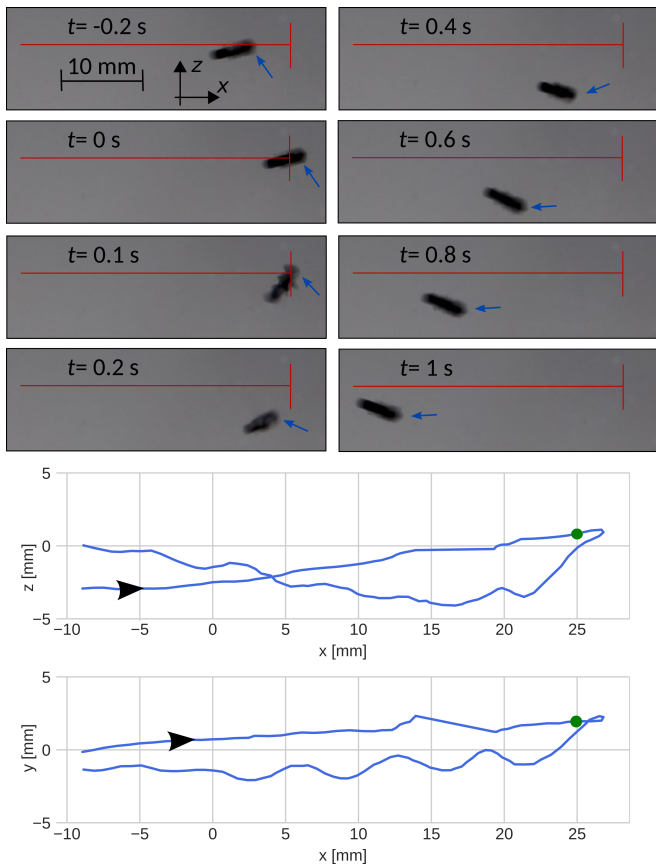


Fig. 8. Frames from the video and plot of the experimental trajectory obtained while performing a direction reversal maneuver. The fore side of the swimmer is indicated by a blue arrow. The green dot indicates the position when the maneuver starts. The reference trajectory is  $z = y = 0$ .

of the rotational speed of the magnetic field plane to a constant value, set to  $15,000 \text{ rad/s}^2$  in our experiment. The rotational direction of the swimmer must be reversed to keep the swimmer moving in the direction requested by the TP. For this reason, the orientation change request is also sent to the module calculating the rotational speed of the swimmer, which takes care of inverting the rotational direction.

The swimmer was programmed to follow a racetrack-shaped trajectory (see Fig. 4). The orientation was manually reversed using a toggle switch in the LabVIEW graphical interface. A video of this experiment is attached to this paper. Frames from the video as well as a plot of the experimental trajectory are presented in Fig. 10.

### C. Combined direction and orientation reversal

For this maneuver the TP requests both an orientation and a direction reversal. In this case the orientation is flipped but the rotational direction of the swimmer does not change. This produced a  $180^\circ$  change in the heading of the swimmer.

The swimmer was programmed to follow a straight horizontal line and perform a *combined direction and orientation reversal* maneuver at each end until the program is manually stopped. A video of this experiment is attached to this paper. Frames from the video as well as a plot of the experimental trajectory are presented in Fig. 9.

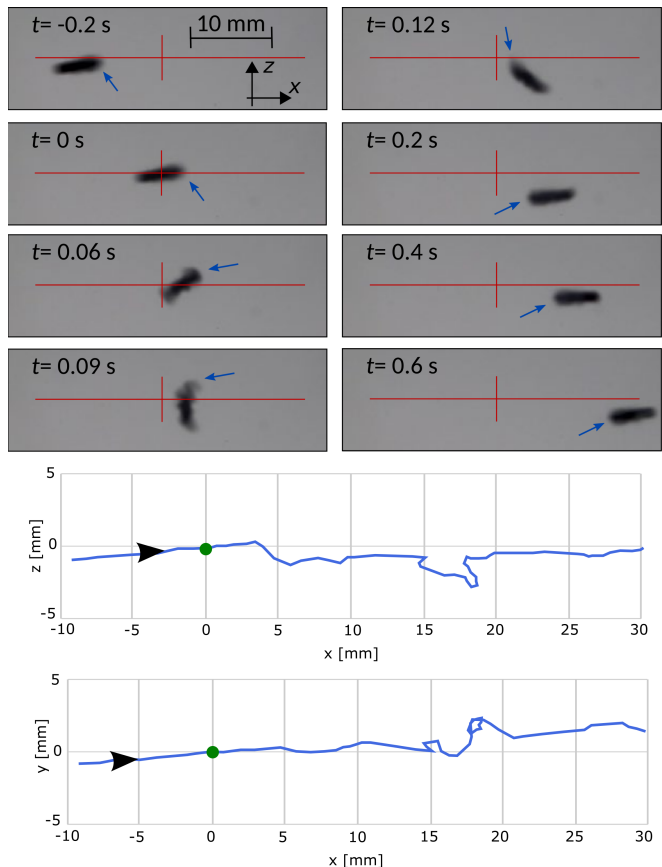


Fig. 9. Frames from the video and plot of the experimental trajectory obtained while performing an orientation reversal maneuver. The fore side of the swimmer is indicated by a blue arrow. The green dot indicates the position when the maneuver starts. The reference trajectory is  $z = y = 0$ .

## V. COMPLEX 3D NAVIGATION

The swimmer was programmed to follow the complex trajectory presented in Fig. 11. This trajectory has a length of 770 mm and includes 10 turns, each having a radius of 7.5 mm. It also includes two direction reversal maneuvers, two orientation reversal maneuvers, and one combined direction and orientation reversal maneuver. A video of this experiment is attached to this paper. The box in the workspace is used to store the swimmer when not used. It ensures that the swimmer starts the navigation close to the beginning of the trajectory to follow. The swimmer was able to successfully follow this complex trajectory with an average position error of 3.8 mm and an average velocity of 54.2 mm/s. This experiment demonstrates that the swimmer is able to follow a complex 3D trajectory with agile maneuvers while revolving inside a liquid having rheologic properties similar to human blood.

## VI. CONCLUSION

Experiments of a magnetic helical swimmer navigating inside a blood-mimicking liquid were presented. These tests aimed at quantifying the maximum turning capabilities of the swimmer. If the maximum torque is exceeded, the swimmer ceases rotating and control is completely lost. The maximum rotational speed was measured as a function of the turning

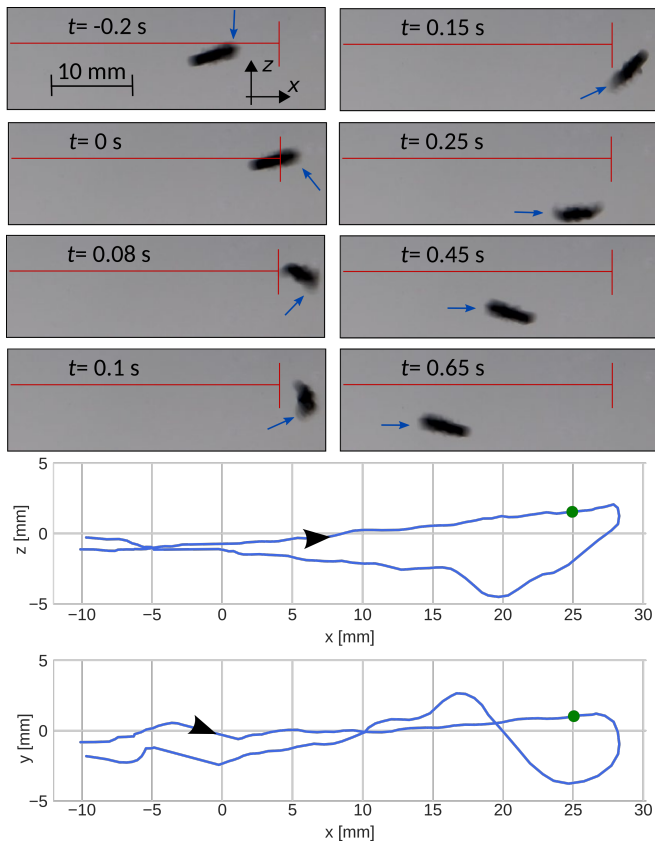


Fig. 10. Frames from the video and plot of the experimental trajectory obtained while performing a combined orientation and direction reversal maneuver. The fore side of the swimmer is indicated by a blue arrow. The green dot indicates the position when the maneuver starts. The reference trajectory is  $z = y = 0$ .

radius. The average positioning error during a turn was also measured.

Three new rapid movements were introduced to increase the swimmer's agility. These maneuvers produce fast modifications of the swimmer's orientation and/or velocity vector. They were tested experimentally and produced deviations of less than 5 mm from the path to follow. The combined direction and orientation reversal produces relatively large position error but could still be useful to negotiate sharp turns in spacious areas as in the heart's right ventricle. The direction reversal could allow changing the direction of motion in a more confined spaces as it does not necessitate a rotation around the radial axis of the agent. The swimmer is, however, less efficient at swimming backward. An orientation change maneuver could be used when enough space is available to rotate the swimmer to the most efficient orientation. This paper also experimentally demonstrated that the swimmer can follow a complex 3D trajectory that includes agile maneuvers. The swimmer performed all the new rapid movements in succession while following a desired path.

More work needs to be accomplished to bring this technology into the clinical realm. Incorporating realistic fluid flow and replacing cameras with a suitable medical imaging technology are the next steps. A cardiac phantom with flow and functional valves would enable studying the control of the swimmer under pulsating turbulent flow. An ultrasound

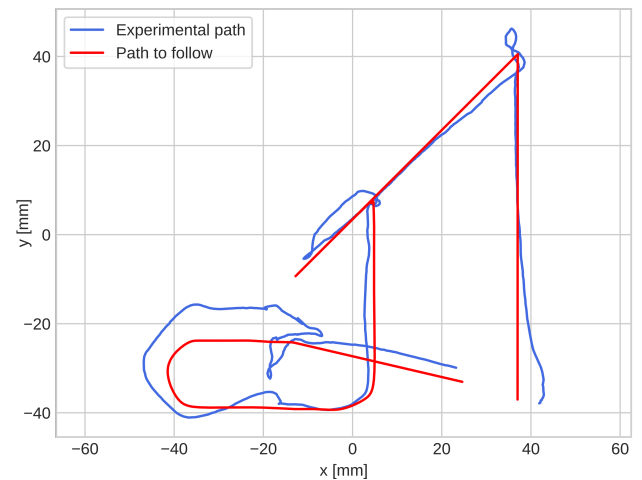
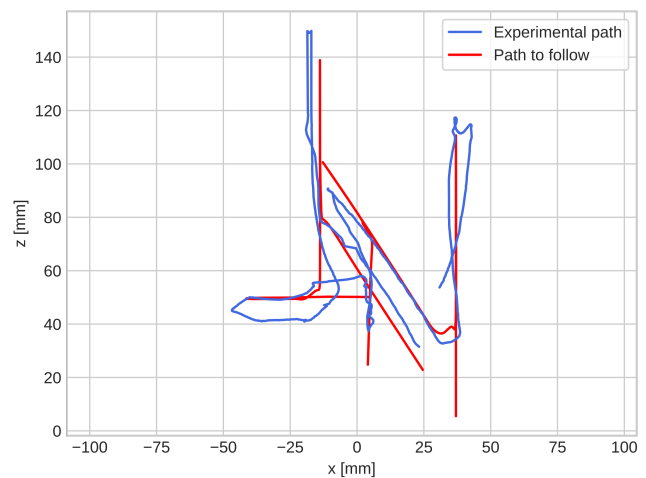
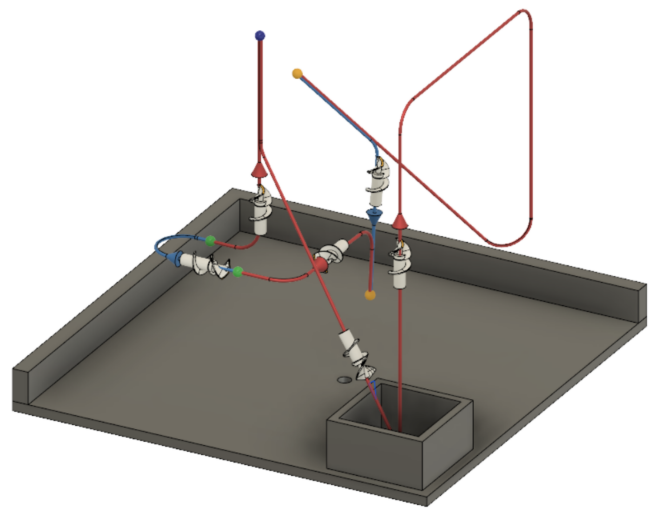


Fig. 11. Top: 3D drawing of the complex 3D trajectory used to test the agility of the swimmer (swimmer not to scale). Plot of the path to follow and the obtained experimental path projected onto the  $x$ - $z$  plane (middle) and the  $x$ - $y$  plane (bottom). The spheres in the 3D drawing indicate the location of a special rapid movement. Yellow spheres correspond to a direction reversal, green spheres to an orientation flip and the blue sphere indicate an combined direction and orientation change. The video attached to this paper shows this experiment.

scanner would not only provide a means for obtaining the swimmer's position inside a patient, but would also enable measuring blood flow via measuring the Doppler effect.

## REFERENCES

- [1] E. Oger, E.-G. study group, *et al.*, "Incidence of venous thromboembolism: a community-based study in western france," *Thrombosis and haemostasis*, vol. 83, no. 05, pp. 657–660, 2000.
- [2] J. W. Eikelboom and J. Hirsh, "Bleeding and management of bleeding," *European heart journal supplements*, vol. 8, no. suppl\_G, pp. G38–G45, 2006.
- [3] N. Kucher, P. Boekstegers, O. J. Müller, C. Kupatt, J. Beyer-Westendorf, T. Heitzer, U. Tebbe, J. Horstkotte, R. Müller, E. Blessing, *et al.*, "Randomized, controlled trial of ultrasound-assisted catheter-directed thrombolysis for acute intermediate-risk pulmonary embolism," *Circulation*, vol. 129, no. 4, pp. 479–486, 2014.
- [4] P. T. Zeni Jr, B. G. Blank, and D. W. Peeler, "Use of rheolytic thrombectomy in treatment of acute massive pulmonary embolism," *Journal of Vascular and Interventional Radiology*, vol. 14, no. 12, pp. 1511–1515, 2003.
- [5] H. Zhao, L. Julien, M. Feucht, O. Bailey, and A. Becker, "3d path-following using mrac on a millimeter-scale spiral-type magnetic robot," *IEEE Robotics and Automation Letters*, 2020.
- [6] T. Xu, G. Hwang, N. Andreff, and S. Régnier, "Planar path following of 3-d steering scaled-up helical microswimmers," *IEEE Transactions on Robotics*, vol. 31, no. 1, pp. 117–127, 2015.
- [7] A. Oulmas, N. Andreff, and S. Régnier, "3d closed-loop swimming at low reynolds numbers," *The International Journal of Robotics Research*, vol. 37, no. 11, pp. 1359–1375, 2018.
- [8] I. S. Khalil, D. Mahdy, A. El Sharkawy, R. R. Moustafa, A. F. Tabak, M. E. Mitwally, S. Hesham, N. Hamdi, A. Klingner, A. Mohamed, *et al.*, "Mechanical rubbing of blood clots using helical robots under ultrasound guidance," *IEEE Robotics and Automation Letters*, vol. 3, no. 2, pp. 1112–1119, 2018.
- [9] D. Mahdy, R. Reda, N. Hamdi, and I. S. Khalil, "Ultrasound-guided minimally invasive grinding for clearing blood clots: promises and challenges," *IEEE Instrumentation & Measurement Magazine*, vol. 21, no. 2, pp. 10–14, 2018.
- [10] I. S. Khalil, A. F. Tabak, K. Sadek, D. Mahdy, N. Hamdi, and M. Sitti, "Rubbing against blood clots using helical robots: Modeling and in vitro experimental validation," *IEEE Robotics and Automation Letters*, vol. 2, no. 2, pp. 927–934, 2017.
- [11] W. Lee, S. Jeon, J. Nam, and G. Jang, "Dual-body magnetic helical robot for drilling and cargo delivery in human blood vessels," *Journal of Applied Physics*, vol. 117, no. 17, p. 17B314, may 2015. [Online]. Available: <http://aip.scitation.org/doi/10.1063/1.4917067>
- [12] A. W. Mahoney, N. D. Nelson, K. E. Peyer, B. J. Nelson, and J. J. Abbott, "Behavior of rotating magnetic microrobots above the step-out frequency with application to control of multi-microrobot systems," *Applied Physics Letters*, vol. 104, no. 14, p. 144101, 2014.
- [13] P. Eckert and A. J. Ijspeert, "Benchmarking agility for multilegged terrestrial robots," *IEEE Transactions on Robotics*, vol. 35, no. 2, pp. 529–535, 2019.
- [14] J. Leclerc, B. Isichei, and A. T. Becker, "A magnetic manipulator cooled with liquid nitrogen," *IEEE Robotics and Automation Letters*, vol. 3, no. 4, pp. 4367–4374, Oct 2018.
- [15] S. Hund, M. Kameneva, and J. Antaki, "A quasi-mechanistic mathematical representation for blood viscosity," *Fluids*, vol. 2, no. 1, p. 10, 2017.
- [16] L. Dintenfass, *Blood viscosity*. Springer Science & Business Media, 1985.
- [17] R. S. Rosenson, A. McCormick, and E. F. Uretz, "Distribution of blood viscosity values and biochemical correlates in healthy adults." *Clinical Chemistry*, vol. 42, no. 8, pp. 1189–1195, 1996.
- [18] H. Hinghofer-Szalkay and J. Greenleaf, "Continuous monitoring of blood volume changes in humans," *Journal of applied physiology*, vol. 63, no. 3, pp. 1003–1007, 1987.
- [19] J. Leclerc, H. Zhao, and A. T. Becker, "3d control of rotating millimeter-scale swimmers through obstacles," in *2019 International Conference on Robotics and Automation (ICRA)*, May 2019, pp. 8890–8896.
- [20] <https://youtu.be/U79idzMZn9Y>.